Colloid & Polymer Science Colloid Polym Sci 272:36–47 (1994)

Isotactic polystyrene/cis-decaline mixtures: phase diagram and molecular structures

J. M. Guenet[1]), A. Menelle[2]), V. Schaffhauser[1,3]), P. Terech[3]), and A. Thierry[4])

[1]) Laboratoire d'Ultrasons et de Dynamique des Fluides Complexes*), Université Louis Pasteur-CNRS URA 851, Strasbourg, France
[2]) Laboratoire Léon Brillouin, CEA-CNRS, CEN Saclay, Gif-sur-Yvette, France
[3]) Institut Laue-Langevin, Grenoble, France
[4]) Institut Charles Sadron (CNRS), Strasbourg, France

Abstract: Organized structures grown from iPS/*cis*-decalin solutions (ranging from 5% to 50% w/w) have been studied by several techniques. From DSC experiments the thermal behavior has been investigated as a function of the annealing temperature. The temperature-concentration phase diagram has been established. From neutron diffraction experiments the short range molecular order has been determined. We show that between the gel state formed at high undercooling and the crystalline state obtained at low undercooling there exist two intermediate phases: the *s-phase*, already described by Klein et al., and the *p-phase*. Except for the crystalline state all the other phases contain intercalated solvent molecules. The *gel* state displays nematic-like order, whereas the *s-phase* is reminiscent of smectic arrangements. The *p-phase* is less solvated and can be described as a peritectic system. Preliminary neutron scattering experiments show that chain-folding reappears in the *s-phase*, whereas it was shown to be absent in the *gel phase*.

Key words: Isotactic polystyrene – cis-decalin – phase diagrams – neutron diffraction – non-crystalline phases

Introduction

The gelation phenomenon of isotactic polystyrene has received continuous attention over the past 15 years [1–5]. Originally, it was thought that there was a competition between gelation and crystallization [2–4]. To achieve the former it was said that the latter had to be by-passed by a rapid quench. This suggested that, starting from solutions at high temperatures, low cooling rates would rather yield a suspension of crystals, whereas high cooling rates would promote gel formation. Correspondingly, this also conveyed the impression that gelation had to be rapid otherwise crystallization would rather prevail.

Recently, Klein et al. [6] have shown that the gel point is a well-defined temperature which appears to be in conflict with the previous statements. As a matter of fact, below the gel point, although gel formation rates are exceedingly slow, only a gel will be produced. If gelation arose from the ordering of chains out of equilibrium then one might expect, in the vicinity of the gel point, to observe both gel and crystals. In addition, these authors have reported that, unlike as was so far claimed, the reappearance of the crystalline state above the gelation point is not systematic. Whereas it was the case with iPS/*trans*-decalin solutions, Klein et al. [6] have conclusively shown the existence of a new state in iPS/*cis*-decalin solutions. This state is not crystalline

*) Formerly Laboratoire de Spectrométrie et d'imagerie Ultrasonores

and is rather reminiscent of smectic-F arrangements, that is, giving lamellar morphology but with low-range molecular order.

The purpose of this paper is to report on studies carried out on iPS/*cis*-decalin solutions in the range of annealing temperatures 20° to 55 °C. We will show that in this range another phase, intermediate between the one discovered by Klein et al. [6] and the crystalline state, exists. After establishing the temperature-concentration phase diagram, neutron diffraction experiments will allow one to unveil the molecular structure. It will be particularly shown that the way solvent molecules intercalate between individual chains determines the existence of these non-crystalline phases.

Experimental

Materials

All isotactic polystyrene samples, hydrogenated and deuterated, were synthesized following the method described by Natta [7]. As ascertained by ^{13}C NMR, polystyrene samples were over 98% isotactic. Molecular weight fractionation was achieved with toluene/ethanol at 30 °C. Molecular weight characterization was carried out in THF with columns calibrated by means of atactic polystyrene standards and using the universal calibration procedure. The samples used in this study together with their molecular weight characteristics obtained by GPC in THF are as follows:

iPSD 3 $M_w = 3 \times 10^5$ $M_w/M_n \simeq 1.35$

iPSD 7 $M_w = 1.25 \times 10^5$ $M_w/M_n \simeq 1.23$

iPSH $M_w = 2.64 \times 10^5$ $M_w/M_n \simeq 1.59$

Cis-decalin, either hydrogenated or deuterated, was purchased from Aldrich and was used without purification. The deuterated *cis*-decalin was over 99% deuterium-labelled.

Sample preparation

DSC: Homogeneous iPS/*cis*-decalin solutions were first obtained in hermetically sealed test tubes by heating above 170 °C. These solutions were quenched to 0 °C in order to produce a gel. Approximately 10 mg of this gel were placed into a "volatile sample" pan. The pan was then heated at 170 °C so as to again produce solutions. Finally, the DSC pan was directly introduced into a special container immersed in a thermostatic bath held at the desired temperature to within 0.1 °C so as to achieve annealing.

Neutron diffraction: The samples were prepared in quartz tubes of inner diameter 3 mm. The iPS/*cis*-decaline mixture was directly prepared in the tube, the latter being hermetically sealed prior to dissolution. By heating above 170 °C solutions were produced that were eventually cooled and subsequently annealed in the aforementioned thermostatic bath at the desired temperature.

Neutron scattering: The solutions were prepared at 170 °C in an air-tight syringe and then gently injected at 100 °C into a rectangular quartz cell of 1-mm thickness. Under these conditions solvent evaporation was negligible. These cells were then hermetically sealed, heated above 170 °C to reform the solution, and finally cooled and annealed as described above.

Techniques

DSC: A differential scanning calorimeter, DCS 4, from Perkin-Elmer was used in this study. Temperature and enthalpy calibration was achieved with indium. Heating rates ranging from 5 °C/min to 20 °C/min were used. The data were processed with the TADS system (Thermal Analysis Data Station).

Neutron diffraction: The neutron diffraction measurements were taken at Laboratoire Léon Brillouin (Saclay, France) on G-6-1, a two-axis spectrometer equipped with a banana-type BF_3 detector composed of 400 cells. The angular resolution was 0.2°. G-6-1 operates with a wavelength of $\lambda = 0.47$ nm which gives the following available q-range:

$2 < q(\text{nm}^{-1}) < 25$ with

$q = 4\pi/\lambda \sin(\theta/2)$ (λ in nm)

in which θ is the scattering angle.

To minimize noise and air scattering all the measurements were carried out with the sample and the neutron beam held under vacuum. Cell efficiency was corrected by using the spectrum of

a vanadium sample. No absolute calibration was attempted as we were primarily interested in the position of diffraction maxima.

Neutron scattering

Small-angle neutron scattering measurements were taken at the ILL (Grenoble, France) on D11 and D17 cameras. By rotating the D17 camera of about 10° the avilable q-range was:

$$0.12 < q\ (\mathrm{nm}^{-1}) < 2.12\ .$$

On D11 by using different sample-detector distances the accessible q-range was:

$$0.05 < q\ (\mathrm{nm}^{-1}) < 1.5\ .$$

The scattered intensity was corrected for sample thickness and transmission and normalized by means of an incoherent *cis*-decalin spectrum, as follows:

$$I_N(q) = \frac{\dfrac{I_s(q)}{T_s\delta_s} - \dfrac{I_0(q)}{T_0\delta_0}}{\dfrac{I_d(q)}{T_d\delta_d} - \dfrac{I_{ec}(q)}{T_{ec}\delta_{ec}}} \qquad (1)$$

in which $I_s(q)$ is the labeled species intensity, $I_0(q)$ the background intensity; $I_d(q)$ the intensity scattered by a 1 mm-*cis*-decalin sample and $I_{ec}(q)$ the scattering by the empty cell; δ and T, with the appropriate subscript, stand for the thickness and for the transmission of the different samples. Under these conditions, $I_N(q)$ reads:

$$I_N(q) = KC_D S(q)\ , \qquad (2)$$

where $S(q)$ is the structure factor of the labeled species and C_D their concentration. K is a constant which is expressed as:

$$K = (a_D - y_D a_H)^2 \times [4\pi\delta_d N_A T_d / g(\lambda)(1 - T_d) m_D^2]\ , \qquad (3)$$

where a_D and a_H are the scattering amplitudes of the labeled species and of the unlabeled species, respectively, m_D the monomer molecular weight, y_D the ratio of the molar volumes of the labeled and unlabeled species ($y_D = v_D/v_H$), N_A Avogadro's number and $g(\lambda)$ a correction factor which mainly depends upon both the neutron wavelength and the spectrometer's type. In the present case experimentally determined values of $g(\lambda)$ are provided in reference [8] for D11 and D17 cameras.

For systems wherein the labeled species are diluted enough, $I_N(q)$ eventually reads:

$$I_N(q) = KC_D M_w P_D(q)\ , \qquad (4)$$

in which M_w and $P_D(q)$ are the weight-average molecular weight and the form factor of the labeled species, respectively.

Results and discussion

As will be gradually apparent by reading this paper, the structures formed in this solvent are mostly non-crystalline although organized. Here, by crystalline it is meant *long-range three-dimensional order*. In most cases the order will not comply to this definition. As a result, these non-crystalline structures will be designated as organized structures throughout.

Thermal behavior

As has been already underlined by Klein et al. [6], annealing times are exceedingly long above 20 °C. Maximum completion of the formation of the organized structures is achieved after a minimum of 1 week annealing. Whereas the amount of organized structures increases with increasing annealing time, their melting point remains virtually unchanged.

After description of the experimental results, use will be made in the discussion of Gibbs phase rule to establish possible and plausible phase diagrams. It is now known that this rule can be applied to a first order approximation to macromolecular systems as emphasized by Sotckmayer et al. [9] and several experimental studies [10–12].

Throughout this thermal investigation the hydrogenated sample (iPSH) has been used. Typically, two types of behavior are observed depending on the annealing temperature T_{an} (Fig. 1):

*for $20\,^\circ\mathrm{C} < T_{an} < 31\,^\circ\mathrm{C}$

the DSC traces display one relatively-sharp endotherm at $50\,^\circ\mathrm{C} \pm 2\,^\circ\mathrm{C}$.

*for $T_{an} > 33\,^\circ\mathrm{C}$

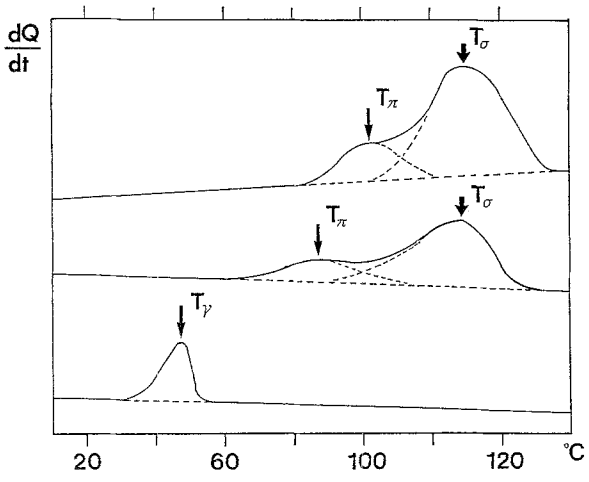

Fig. 1. DSC traces for samples annealed between 20° to 31 °C (lower curve) and between 33° to 55°C (middle curve and upper curve). The upper curve corresponds to samples annealed above 45°C. T_γ is the melting of the polymer-solvent compound, T_π the peritectic transformation, and T_σ the final crystal melting. In the present case heating rate is 10°C/min, iPSH sample with $C = 30\%$ for the lower curve and $C = 35\%$ for the middle and the upper curves

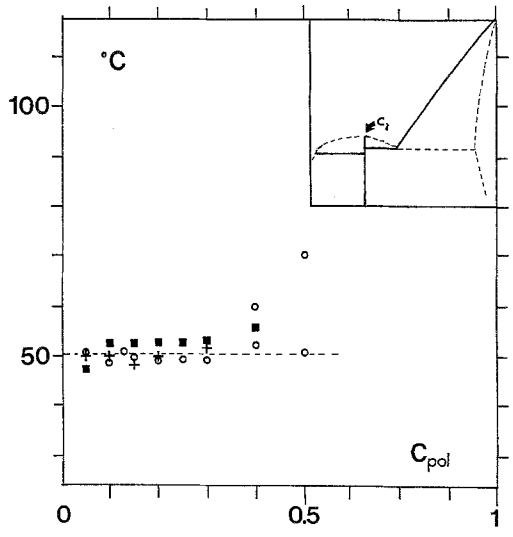

Fig. 2. Temperature-concentration phase diagram obtained for samples annealed below $T_{an} = 31$°C: ■ = $T_{an} = 23$°C; ○ = $T_{an} = 27$°C; + = $T_{an} = 29$°C. Heating rate = 10°C/m, iPSH sample. Inset: possible theoretical phase diagram corresponding to these results. As usual the dashed lines correspond to what might be normally expected from phase rules but which is not experimentally known

the DCS thermogram exhibits two relatively-broad endotherms. The position as well as the width of these endotherms are sensitive to the annealing temperature: annealing between 34° to 45°C gives a lower endotherm at 85°C, whose position is independent of polymer concentration; annealing above 45°C shifts this endotherm to 100°C. The high-melting endotherm shifts also by about 15°C, yet its position depends upon polymer concentration.

The domain between 31° and 33°C is a kind of transition zone as one can observe a combination of these two types of behavior. We shall return later to this point. Suffice it to note presently that, within a very narrow range of temperature, a dramatic change is seen on the thermal behavior of these polymer-solvent mixture, which is most unusual.

Temperature domain 20°C to 31°C

In Fig. 2 is drawn the temperature-concentration phase diagram obtained on melting at 10°C/min samples annealed between 20 to 31°C. As can be seen, the melting point, which lies at $T_\gamma = 50$°C ± 2°C, does not vary in a large range of concentration. This temperature is not sensitive to the annealing time and little sensitive to the heating rate in the range 5°C/min to 20°C/min. Significant departure from this behavior is seen for polymer concentration over $C_{pol} = 30\%$. For $C_{pol} = 40\%$ and 50% two endotherms can be observed (not shown here), the position of the highest one being dependent upon polymer concentration. These results are much reminiscent of what has been obtained with the same solutions quenched below 20°C whereupon a gel is produced [6].

The variation of the melting enthalpy corresponding to T_γ vs polymer concentration (ΔH_γ) is drawn in Fig. 3. The variation does not show any significant dependence with heating rate nor with the annealing temperature. ΔH_γ exhibits a maximum near $C_{pol} = C_\gamma = 30\%$, which concentration should correspond to the stoichiometric concentration. The value reached by the melting enthalpy at this concentration is about $\Delta H_\gamma \simeq 1.2$ cal/g. As is the case for the gel state this behavior hints at the existence of a polymer-solvent compound with a virtually-identical stoichiometry [5]. Yet, the value of the melting enthalpy at the stoichiometric composition is

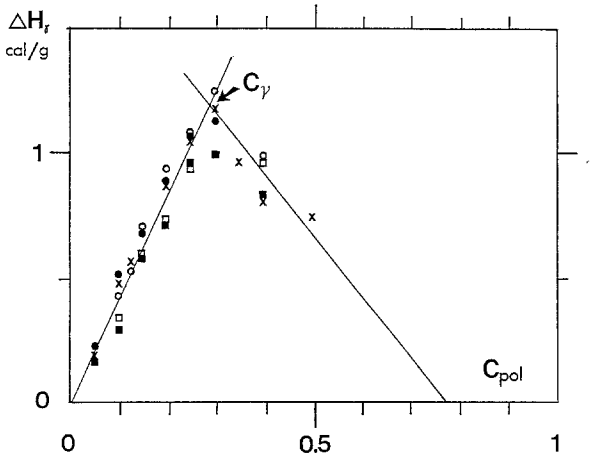

Fig. 3. Plot of the melting enthalpy, ΔH_γ, of the species grown for $T_{an} < 31°C$ as a function of iPSH concentration and for different heating rates: ■ = $T_{an} = 27°C$ and 20°C/m; □ = $T_{an} = 29°C$ and 20°C/m; $T_{an} = 23°C$ and 20°C/m = ○, 10°C/m = ×, 5°C/m = ●. C_γ defines the stoichiometric composition

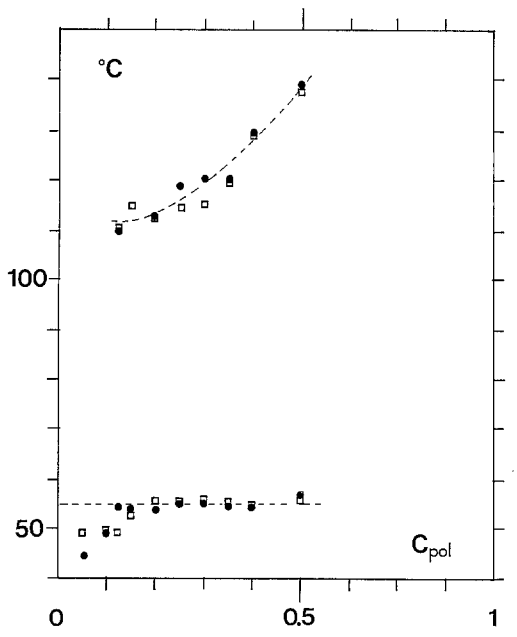

Fig. 4. Temperature-concentration phase diagram for samples annealed between 31° and 33°C. $c = 31°C$ and $o = 33°C$. As usual, the dashed lines correspond to what might be normally expected from phase rules but which is not experimentally known

significantly lower in the gel state ($\Delta H_\gamma \simeq 0.9$ cal/g[5]). This may possibly indicate the presence of more non-organized material in the gel state.

In the inset of Fig. 2 is drawn a plausible schematic phase diagram corresponding to the case studied here. For $C_{pol} < 30\%$ the system is constituted of *compound + liquid*, whereas for $C_{pol} > 30\%$ the system is composed of *compound + solid solution*. Worth noting is that for a semi-crystalline polymer whenever there is solvent located in the amorphous domain the system may be regarded as a *solid solution*.

Temperature domain 31°C to 33°C

As said above this domain is a transition domain as both type of behavior can be observed (Fig. 4), although the endotherms corresponding to the second type are rather weak. Further, the low-melting endotherm is now located at 55°C ± 2°C.

The presence of three melting endotherms (not shown here since it is simply a superimposition of what is seen below 31°C and above 33°C with endotherms located at 55°C, 85°C, and above 100°C depending on concentration), which implies the existence of three stable, organized phases apparently violates Gibbs phase rule for a two-component system (three phases can only coexist at a point of fixed concentration and temperature). A possible and generally admitted explanation to the existence of such a transition domain instead of a sharp, well-defined transition might be sought in molecular weight polydispersity (here $M_w/M_n \approx 1.59$).

Temperature domain > 33°C

The temperature-concentration phase diagram is drawn in Fig. 5. As can be seen the position of the lower melting endotherm as determined after deconvolution (see Fig. 1) does not vary with polymer concentration. For annealing temperatures below 45°C it stands at $T_\pi = 85°C \pm 5°C$ and increases up to $T_\pi = 100°C \pm 1°C$ for annealing temperatures higher than 45°C. Conversely, the position T_σ of the high-melting endotherm increases with polymer concentration and, as expected, is, as a rule, shifted toward higher temperatures for higher annealing temperature, an effect much reminiscent of what takes place in the bulk-state [13]. The experimental

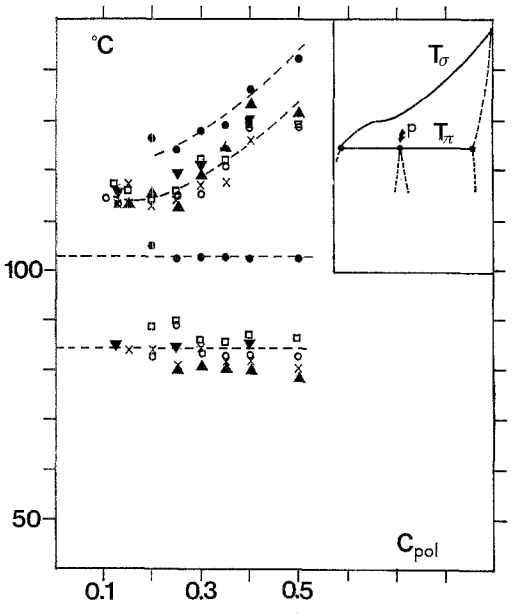

Fig. 5. Temperature-concentration phase diagram for samples annealed above 33°C. ▼ = T_{an} = 35°C; ▲ = T_{an} = 38°C; × = T_{an} = 41°C; ○ = T_{an} = 43°C; □ = T_{an} = 45°C; ● = T_{an} = 55°C. Sample iPSH heating rate 20°C/m. Inset: possible theoretical phase diagram corresponding to these results. As usual, the dashed lines correspond to what might be normally expected from phase rules but which is not experimentally known

scatter observed for samples annealed below 45 °C arises most probably from the difficulty in determining precisely the maximum of the endotherm. When this endotherm is sharper, as is the case with samples annealed above 45°C, the determination becomes much easier and the scatter becomes far less important.

The high-melting endotherm variation follows the behavior predicted by Flory's relation for the melting point depression ΔT [14]:

$$\frac{\Delta T}{T_\sigma \times T^0_{m_p}} = \frac{RV_m}{\Delta H_{0_p} \times V_s}[(1 - v_p) - \chi_1(1 - v_p)^2], \quad (3)$$

in which T_σ and $T^0_{m_p}$ are the actual melting point of the solid solution and of the pure polymer, $\Delta T = T^0_{m_p} - T_\sigma$, V_s and V_m the molar volumes of the solvent and the monomer, respectively, v_p the polymer volume fraction, χ_1 the Flory's parameter of interaction and ΔH_{0_p} the melting enthalpy of the pure polymer. For $0.4 < \chi_1 < 0.5$ and $180°C < T^0_{m_p} < 200°C$, which are usual values for polystyrene [13], good agreement is obtained to within $\pm$ 5°C.

The variation of the enthalpy associated with the low-melting endotherm, ΔH_π, displays a maximum near $C_{pol} = 35\%$ unlike the enthalpy corresponding to the high-melting endotherm which increases continuously instead (Fig. 6). In the latter case the extrapolated value for $C_{pol} = 1$ amounts to $\Delta H_\sigma = 6.1$ cal/g. Assuming that this endotherm corresponds to the fusion of usual iPS crystals, then, by taking $\Delta H_{cry} = 18.3$ cal/g, one can derive a degree of crystallinity of about 33%, a figure quite consistent with values reported in the literature [13, 15].

This type of thermal behavior can be accounted for by considering a peritectic transformation with a peritectic composition $C_\pi = 35\%$ (see inset of Fig. 5). Interestingly enough, a peritectic is closely related to an incongruently melting compound. This implies that solvent molecules are

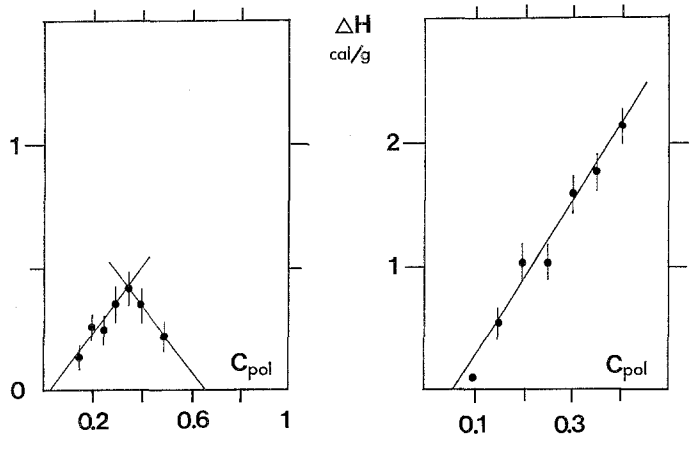

Fig. 6. Plot of the enthalpy corresponding to the low-melting peak, after deconvolution (right) and the high melting peak (left) as a function of polymer concentration. The values correspond to averaged values obtained at different temperatures (between 35° to 45°C). Error bars stand for the experimental scatter

still occluded in the organized domains. At T_π desolvation most probably occurs which gives off the semi-crystalline state, the ultimate stable state before complete melting at T_σ. In this case, it is indeed expected that T_σ be dependent upon concentration.

It is worth adding that these two endotherms are not related to any fusion-recrystallization phenomena as have been observed in the bulk state [16, 17]. When such recrystallization process occurs, the ratio between the areas of the two endotherms is exceedingly sensitive to the heating rate. Here, we have examined a 35%-sample annealed at 45°C at heating rates 20°C/m, 10°C/m, and 5°C/mn. The ratio between the endotherm was seen to vary very little and can be regarded as nearly constant within experimental uncertainties (4.1 ± 0.5, 3.3 ± 0.4 and 3.6 ± 0.4, respectively).

The results obtained at different annealing temperatures can be used to establish a tentative *formation phase diagram* which is drawn in Fig. 7. As is usual in establishing phase diagrams, the heavy lines stand for the transitions known to be certain, whereas the dotted line indicate possible extensions.

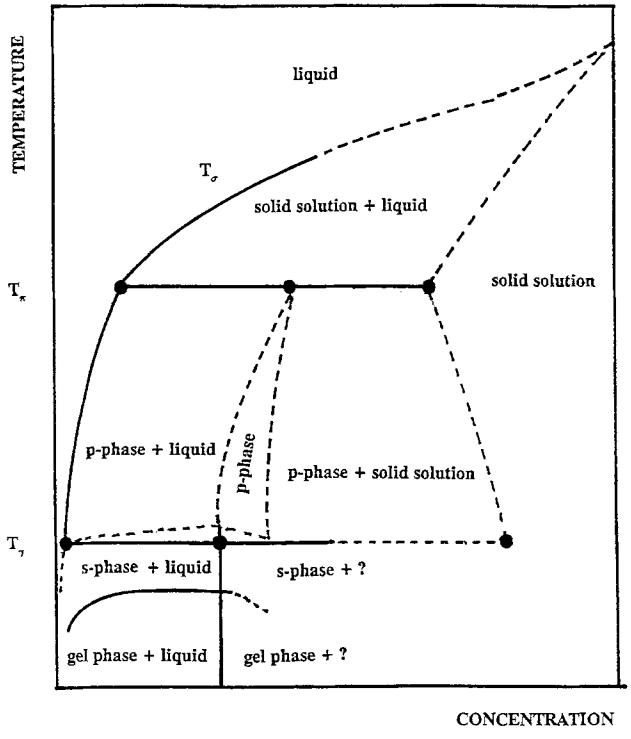

Fig. 7. Possible formation phase diagram for the system iPS/*cis*-decalin. As usual, the heavy lines stand for experimentally determined transition while dashed lines indicate possible extensions

Molecular organization

Neutron diffraction: Samples containing deuterated isotactic polystyrene (iPSD7) with hydrogenated *cis*-decalin have been investigated. This enables one to increase the diffraction power of the polymer with respect to the solvent and, accordingly, determine the polymer-polymer correlations. This study has been restricted to concentrations, as determined from the phase diagrams, corresponding to the polymer-solvent compound stoichiometry for samples annealed below 30°C ($C_\gamma = 30\%$) and to the peritectic composition for samples annealed above 35°C ($C_\pi = 35\%$).

As has been already reported in a previous paper [6] large distances (> 1 nm) are dealt with. As a result, diffraction is smeared by rod scattering. A plot of the type $q^n I(q)$ vs q proves to be more appropriate to highlight the diffraction maxima. In the present case $n = 0.7$ has been arbitrarily used for the sake of the figure's clarity. The data are given in Fig. 8 by means of this representation.

As can be seen, there is a diffraction maximum at $q = 2.65 \pm 0.03\ \text{nm}^{-1}$ ($d = 2.37 \pm 0.03$ nm as calculated with Bragg's law) for the gel (8a), the

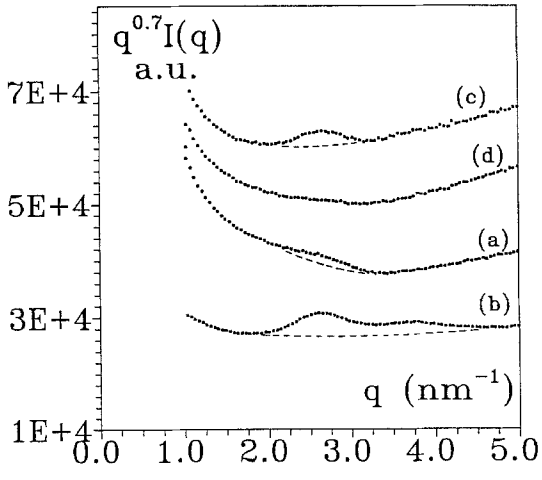

Fig. 8. Neutron diffraction data plotted as $q^{0.7} I(q)$ in arbitrary units vs q in nm^{-1}. a = gel state ($C_{pol} = 30\%$); b = samples annealed between 20° and 31°C ($C_{pol} = 30\%$); c = sample annealed at 35°C ($C_{pol} = 35\%$) and d = same as c but further annealed at 100°C for 2 h ($C_{pol} = 35\%$)

system annealed at 25°C (8b) and the system annealed at 35°C (8c). For samples annealed at 25°C there is an additional maximum at $q = 3.8 \pm 0.03\ \text{nm}^{-1}$ ($d = 1.65 \pm 0.03$ nm) as already reported by Klein et al. [6]. The maximum at $q = 2.65\ \text{nm}^{-1}$ observed in the gel state is poorly defined when compared to the ones obtained at annealing temperatures of 25° and 35°C. Finally, once the sample annealed at 35°C has been further annealed at 100°C to achieve the peritectic transformation, the maximum at $2.65\ \text{nm}^{-1}$ vanishes (Fig. 8d). Correspondingly, one retrieves at large angles diffraction maxima, although admittedly weak, due to usual iPS 3_1 crystals [18] (not shown here). These maxima are not visible in the other samples, except the one at 1.1 nm for the sample annealed at 25°C.

The schematic structures drawn in Fig. 9 are considered here to account for the above data. In all cases, except for the crystalline state, intercalated solvent is present. Solvent intercalation is based on recent investigations and conclusions by

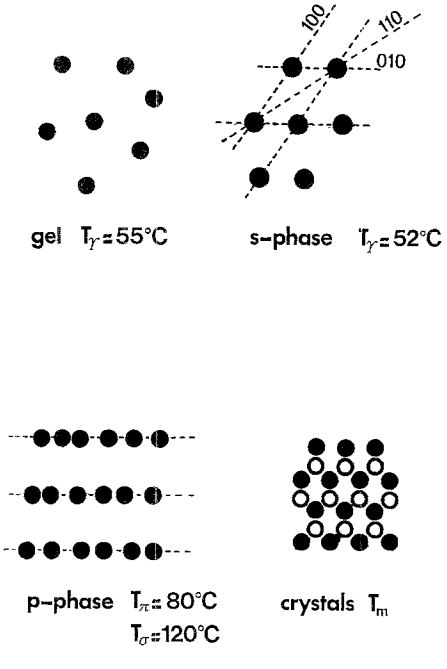

Fig. 9. Possible molecular arrangements as deduced from the neutron diffraction data and the DSC results. Dots correspond to rods as seen parallel to their axis. There are solvent molecules when the rods are spaced apart. For the sake of clarity the solvent molecules are not represented. In the case of the crystalline state filled dots and open dots are used so as to differentiate right- and left-handed helices

Klein et al. [6]. Since the order between solvent molecules is most probably liquid-like they are not represented in the models of Fig. 9 for the sake of clarity. Also, it is considered that the helical form is the *near-*3_1 *form* for the solvated phases and, obviously, the 3_1 *form* for the semi-crystalline state. Details about the choice of a *near-*3_1 *form* can be found in reference [6] and will, accordingly, not be further discussed here.

The *gel state* is reminiscent, as has been already discussed elsewhere, of a nematic state which means that chains are parallelly arranged with no further order. Accordingly, the diffraction maximum is related to the distance between first neighbors. This distance is given by the first maximum of the radial distribution function perpendicular to the rods which can be, in principle, derived from the cylindrical Fourier transform (also called Hankel transform) of the intensity. Yet, in the present case it is not possible to properly calculate this function. Consequently, we shall use the following approximate relation which holds for cylindrically-averaged systems [19, 20]:

$$1.116\lambda \simeq 2d \sin\theta/2\ . \tag{4}$$

From the maximum at $q = 2.65 \pm 0.09$ nm, we derive $d \simeq 2.6 \pm 0.09$ nm. This figure is consistent with the ladder-like model [21] together with the degree of solvation as determined by other methods. Indeed, it is said that about two decaline molecules are bound per monomer. As the size of one molecule is about 0.5 nm, the minimum distance between two monomers solvated each by two solvent molecules can be estimated to be about 2 nm.

The structures grown between 20° and 31°C are evidently more ordered, as already claimed by Klein et al. [6]. Here, we suggest a two-dimensional rhombohedric lattice of rods with $a = 2.96$ nm, $b = 2.054$ nm and the angle $\gamma = 125.8°$. This model should give reflections for the 100, 010, and 110 planes corresponding to 2.5 nm, 1.6 nm, and 1.1 nm. These distances are in agreement with the experimental ones within experimental uncertainties. We surmise that lattices are rapidly decorrelated, which accounts for the low number of reflections. On account of its similarity with smectic arrangement, we shall designate this structure as the *s-phase*. Basically, the

s-phase is simply a more ordered form of the gel structure.

Above 33 °C, the structure designated as *p-phase* is liable to account for the disappearance of the reflections at 1.65 nm and 1.1 nm. Here, the structures are depicted as an assembly of parallel sheets, separated by a distance $d = 2.37$ nm, which is made up of stacked rods with no well-defined spacing as solvent molecules are possibly still occluded within. This arrangement may be thought to correspond to the *s-phase* once solvation in the 010 planes has decreased while being virtually unaffected in the 100 plane. The occurrence of a less solvated phase is borne out by the DSC results which indicate that the peritectic composition is 1.4 solvent molecule/monomer ($C_\pi = 0.35$) against 1.9 molecule/monomer in the *s-phase* ($C_\gamma = 0.3$).

Finally, the structures produced by annealing first at 35 °C then at 100 °C correspond simply to the usual crystalline state [22]. Here, left-handed and right-handed helices are differentiated.

Neutron scattering: It is worth testing these models by investigating the scattering of similar samples at small-angles. As a matter of fact, the intensity scattered by parallel cylindrical objects of infinite length reads [23]:

$$S(q) = s(q)\left\{1 - v\int_0^\infty 2\pi(1 - g(r))\,J_0(qr)\,r\,dr\right\}, \tag{5}$$

in which v is the number of rods per unit area, $g(r)$ the radial distribution function of the rods and $J_0(qr)$ the Bessel function of first kind and order 0. $s(q)$ is the form factor of an infinite rod of cross-sectional radius r_c and of linear mass μ_L [24]:

$$s(q) = \{\pi\mu_L/q^3 r_c^2\} \times J_1^2(qr_c)\,, \tag{6}$$

in which J_1 is the Bessel function of first kind and order 1.

If d is the average distance between first neighbors and provided $d > r_c$, then for $ql_c > 1$ (l_c = lamellar thickness) for $qd > 1$ and $qr_c < 1$ $g(r) \approx 0$, relation (5) can be approximated to:

$$S(q) = (\pi\mu_L/q) \times \exp - q^2 r_c^2/2\{1 - v2\pi q^{-0.5} f(r)\}\,, \tag{7}$$

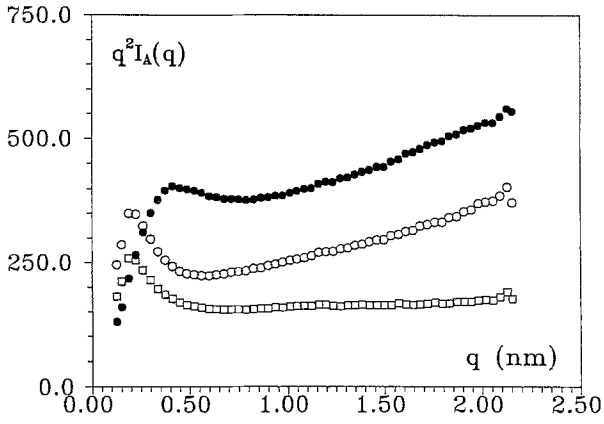

Fig. 10. Small-angle neutron scattering data ($q^2 I(q)$ in absolute units vs q in nm^{-1}) on samples containing only deuterated polymer (sample iPSD3) and hydrogenated solvent. o = gel prepared at 17 °C ($C_{pol} = 30\%$); o = sample annealed at 25 °C ($C_{pol} = 30\%$); c = sample annealed at 35 °C ($C_{pol} = 35\%$)

in which $f(r)$ is an oscillating function whose maxima depend upon the rod arrangement. Relation (7) implies that $S(q)$ will reach, in the range so defined, an asymptote proportional to q^{-1}.

Finally, if the *p-phase* structure is considered, $S(q)$ will read:

$$S(q) = \{2\pi\mu_s/q^2\}\{1 - h(qd)\}\,. \tag{8}$$

The q^{-2} term arises from the sheet-like structure [25], the specific mass of which is μ_S. $h(qd)$ is an interference function between the sheets. For $qd > 1$, $h(qd)$ can be neglected so that $S(q)$ is expected to reach a q^{-2} behavior.

No numerical fit has been attempted, only the terminal behavior has been evaluated. Small-angle neutron scattering results obtained on the *gel phase*, the *s-phase* and the *p-phase* are in qualitative agreement with the molecular models as deduced from neutron diffraction maxima (see Fig. 10).

As can be seen by means of a Kratky representation ($q^2 I(q)$ vs q), one observes a pronounced upturn at large angles for the *gel phase* and the *s-phase* which is expected from relation (7). Also, the patterns in both cases are much the same which gives further support to the similarity between both phases. The fact that the intensity is lower in the case of *s-phase* hints at stronger interferences and, correspondingly, at a better organization here.

Concerning the *p-phase* a q^{-2} behavior is observed beyond $q^* > 0.65\ \mathrm{nm}^{-1}$. By supposing that sheet interferences grow negligible for a spacing whose approximate value is given through $d \simeq 2/q^*$, one obtains an estimate of $d \simeq 3$ nm. This figure is of the right order of magnitude in agreement with the one found above by neutron diffraction ($d = 2.65$ nm).

The smallest angles are worth examining as they may give indications as to the lamellar thickness in the spherulites present in the *s-phase* and the *p-phase*. As can be seen, there is a marked maximum for samples annealed at 25° and 35°C. In a $I(q)$ vs q representation this maximum corresponds to a shoulder (no shoulder is seen in the gel case). If one regards this shoulder as arising from the long-spacing, L_c, between lamellae, then one obtains $L_c \simeq 31.4$ nm. The fact that a shoulder is observed rather than a peak may be due to the poor contrast difference between the organized and the disorganized domains, something which also exists in the case of bulk-crystallized samples [26].

This long-spacing value is larger than what is usually reported in the bulk state [26]. As will be seen in what follows, this may originate in the special chain trajectory occuring under these conditions.

Chain trajectory: Preliminary investigations into the chain trajectory have been achieved by small-angle neutron scattering for samples annealed at 25°C. The scattering pattern obtained is drawn in Fig. 11 by means of a Kratky representation. As can be seen, the q^{-1} behavior can be identified at small angle, but also at large angles. Such a pattern can be accounted for by using a twice folded chain (see Fig. 12), designated as *wicket model* in what follows. By neglecting the loops, the intensity of this model reads for $qL > 1$ [23]:

$$I(q) \approx (\pi M/3qL) \times [3 + 4J_0(qd) + 2J_0(2qd)] , \quad (9)$$

in which L is the chain's contour length, M its molecular weight, and d is the distance between the rods and J_0 the Bessel function of first kind and order 0. For $qL > 1$ with $qd < 1$ relation (9) reduces to:

$$I_1(q) \approx (3\pi\mu_L/q) \times \exp - q^2 d^2/3 , \quad (10)$$

which gives an initial slope $I_1(q) \approx (3\pi\mu_L/q)$.

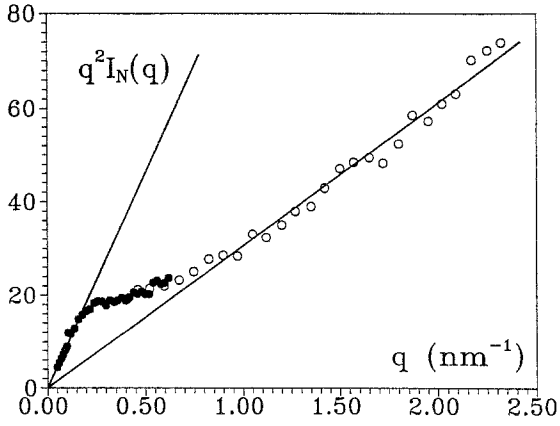

Fig. 11. Small-angle neutron scattering ($q^2I(q)$ in absolute units vs q in nm^{-1}) for deuterated chains ($C_D = 1.89 \times 10^{-2}$ g/cm^3) in a sample annealed at 25°C of total polymer concentration $C_{pol} = 30\%$. Full circles and open circles stand for two different sample-detector distances on D11 camera and straight lines define the two different q^{-1} regimes

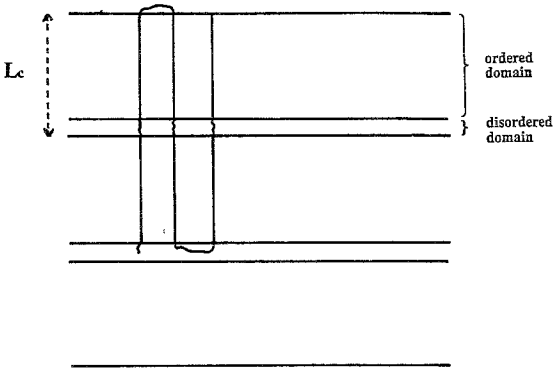

Fig. 12. *Wicket model* model for a chain twice-folded and going through several lamellae

For $qL > 1$ together with $qd > 1$ the Bessel function can be approximated to:

$$J_0(x) \simeq \left(\frac{2}{\pi x}\right)^{1/2} \times \cos[x - \pi/4] . \quad (11)$$

The intensity then reads:

$$I_2(q) \approx \pi\mu_L/3q\left(3 + \frac{2}{(\pi qd)^{0.5}}\sigma(qd)\right), \quad (12)$$

wherein $\sigma(qd)$ is an oscillating function which reads:

$$\sigma(qd) = 2\sqrt{2}\cos(qd - \pi/4) + \cos(2qd - \pi/4) . \quad (13)$$

The second member in the bracket of 12 becomes rapidly unimportant so that $I_2(q) \approx \pi\mu_L/q$. The ratio of the initial slope of $I_1(q)$ to the terminal slope of $I_2(q)$ in the Kratky representation should then amount to about 3 which is experimentally obtained.

Interestingly enough, the linear mass μ_L determined from the experimental intensity $I_2(q)$ amounts to $\mu_L \simeq 520 \pm 50$ g/mole × nm, a figure which agrees better with a *near*-3_1 *form* than with a 12_1 *form* (for deuterated chains $\mu_L(3_1) = 505$ g/mole × nm while $\mu_L(12_1) = 440$ g/mole × nm).

It is worth emphasizing that, provided the chain takes on a *near*-3_1 form, each branch of the *wicket model* goes through several lamellae: for the molecular weight involved here, the length of a branch is about 80 nm to be compared with the estimated long spacing of 31.4 nm. To have the rigidity as revealed by neutron scattering maintained over two lamella may suggest that the disordered region is rather small compared to the organized one. This suggestion might explain why the spherulites are so large (diameter $\simeq 180$ μm) despite the absence of long-range order between chain segments.

Determination of the conformation on either side of the gel point shows that the difference between the *gel phase* and the *s-phase* not only occurs at short-range distances, but also on the chain conformation. Chain-folding exists in the *s-phase*, although not to the extent observed in the semi-crystalline state [27], while it is absent in the *gel phase*. This probably explains why *gel* morphology is fiber-like, whereas *s-phase* morphology is spherulitic [3, 6].

The gel point would then appear to some extent as the limit between worm-like chains and *wicket-like* chains. This is, reminiscent of the behavior expected for polymeric liquid-crystals [28], for which worm-like to hair-pin transition takes place. However, in the case considered here the transition is first-order (abrupt change between worm-like to wicket-like chains), whereas it is second-order for polymeric liquid crystals and thus described by an Arrhenius-equation in reference [28].

Conclusion

In this paper we have presented results, gathered by different techniques, that all consistently suggest the existence of intermediate phases between the gel state and the semi-crystalline state in iPS/*cis*-decalin systems. As intuitively expected, the gel state, obtained at the highest undercooling, is the less organized one and its molecular organization resembles closely nematic order. Decreasing the undercooling yields a better organized phase (the *s-phase*) and, eventually, a less solvated one (the *p-phase*). At the lowest undercooling one obtains the most ordered one which, does not contain intercalated solvent.

These types of solvated phases are most probably not restricted to isotactic polystyrene. It would not be surprising that some other polymer-solvent systems behave in the same way. One requirement would possibly be the use of polymers possessing bulky side-groups as are the phenyl groups in iPS.

References

1. Lemstra PJ, Challa G (1975) J Polym Sci Polym Phys Ed 13:1809
2. Girolamo M, Keller A, Miyasaka K, Overbergh N (1976) J Polym Sci Polym Phys Ed 14:39
3. Guenet JM, Lotz B, Wittmann JC (1985) Macromolecules 18:420
4. Perez E, Vanderhart DL, McKenna GB (1988) Macromolecules 21:2418
5. Guenet JM, McKenna GB (1988) Macromolecules 21:1752
6. Klein M, Menelle A, Mathis A, Guenet JM (1990) Macromolecules 23:4591
7. Natta G (1955) J Polym Sci 16:143
8. Ragnetti D, Oberthür R (1986) Colloid Polym Sci 264:32
9. Koningsveld R, Stockmayer WH, Nies E (1990) Makromol Chem Macromol Symp 39:1
10. Point JJ, Coutelier C (1985) J Polym Sci Polym Phys Ed 23:231
11. Smith P, Pennings AJ (1974) Polymer 15:413
12. Borchhardt (1990) Makromol Chem Macromol Symp 39
13. Overbergh N, Berghmans H, Smets G (1972) J Polym Sci Pt C 38:237
14. Flory PJ (1953) Principles of Polymer Chemistry. Cornell Univ. Press, Ithaca, NY
15. Overbergh N, Berghmans H, Reynaers H (1976) J Polym Sci Polym Phys Ed 14:1177
16. Lemstra PJ, Kooistra T, Challa G (1972) J Sci Polym Pt A2 10:823

17. Overbergh N, Girolamo M, Keller A (1977) J Polym Sci Polym Phys Ed 15:1475
18. Buchanan DR, Miller RL (1966) J Appl Phys 37:4003
19. Guinier A (1956) Théorie et Technique de la Radiocristallographie. Dunod Paris This relation is derived as follows. The intensity in the case of parrallel rods is $I(q) \approx \sum_i \sum_j J_0(qr_{ij})$. The first neighbors will mostly contribute to the intensity so that the first maximum of $J_0(qd)$ should correspond in a first approximation to the first maximum of the intensity. As J_0's first maximum occurs for $qd = 7.0156$, one obtains relation (4).
20. see also for instance Leadbetter AJ, Richardson RM, Colling CN (1975) J Phys (Les Ulis Fr.) 36: C1-37
21. Klein M, Brûlet A, Guenet JM (1990) Macromolecules 23:540
22. Natta G, Corradini P, Bassi IW (1960) Nuovo Cimento Suppl 15:68
23. Oster G, Riley DP (1952) Acta Cryst 5:272
24. Porod G (1948) Acta Phys Aust 2:255
25. Porod G (1951) Koll Z 124:83
26. Overbergh N, Sadler DM, Keller A (1977) J Polym Sci Polym Phys Ed 15:1487
27. Guenet JM (1981) Polymer 22:313
28. de Gennes PG (1982) In: Polymer Liquid Crystal. Acad Press, NY

Received November 26, 1992;
accepted April 6, 1993

Authors' address:

Prof. J.M. Güenet
ULP
Laboratoire d'Ultrasons et de Dynamique
des Fluides Complexes
URA 851
4, rue Blaise Pascal
67070 Strasbourg, France